Southern Ocean seabird population shifts over the Holocene revealed by peat sequestration of mercury from guano

Chuxian Li [1,2]*, Stephen J. Roberts [3], Martin Grosjean [1], Adrien Mestrot [1], Martin Wille [4], Richard A. Phillips [3], Maxime Enrico [5], Kevin Bishop [2], Ulf Skyllberg [6], Dmitri Mauquoy [7], Clemens von Scheffer [7], Thomas Theurer [7], David Muirhead [7], Alex Whittle [3,8], Angela Gallego-Sala [8], Jeroen E. Sonke [9], François de Vleeschouwer [10], Nathalie Van der Putten [11], Pascale Braconnot [12], Olivier Marti [12], Stefan Osterwalder [13], Nina Buchmann [14], Thomas Frölicher [15], Eva Anthamatten [1], Aurea C. Chiaia-Hernández [1], Petra Zahajská [1], Catherine Jeandel [16], Krystyna M. Saunders [17], Sae Yun Kwon [18], Dingyong Wang [19], Richard Bindler [20], Louise Sime [3], Dominic A. Hodgson [3]

*Corresponding author: chuxian.li@slu.se

Affiliations

1. Institute of Geography and Oeschger Center for Climate Change Research, University of Bern, Bern 3012, Switzerland
2. Department of Aquatic Sciences and Assessment, Swedish University of Agricultural Sciences, Uppsala 75007, Sweden
3. British Antarctic Survey, Natural Environment Research Council, High Cross, Madingley Road, Cambridge, UK
4. Institute of Geological Sciences, University of Bern, Bern, Switzerland
5. Université de Pau et des Pays de l'Adour, E2S UPPA, CNRS, IPREM, Pau 64000, France
6. Department of Forest Ecology and Management, Swedish University of Agricultural Sciences, Umeå, Sweden
7. School Geosciences, University of Aberdeen, Scotland, UK
8. Geography Department, University of Exeter, Exeter, UK
9. EcoLab, Université de Toulouse, CNRS, INPT, UPS, Castanet Tolosan, France
10. Instituto Franco-Argentino para el Estudio del Clima y sus Impactos (UMI 3351 IFAECI/CNRS-CONICET-UBA-IRD), Universidad de Buenos Aires, Argentina
11. Department of Earth Sciences, Vrije Universiteit Amsterdam, Amsterdam, Netherlands
12. Laboratoire des Sciences du Climat et de l'Environnement, LSCE/IPSL, CEA-CNRS-UVSQ, Université Paris-Saclay, Gif-sur-Yvette, France
13. Department of Geography, Hydrology and Climate, University of Zurich, Zurich, Switzerland
14. Grassland Sciences, Institute of Agricultural Sciences, ETH Zürich, Zürich, Switzerland
15. Climate and Environmental Physics, University of Bern, Bern, Switzerland
16. LEGOS, Université de Toulouse, CNES, CNRS, IRD, Toulouse, France
17. Australian Nuclear Science and Technology Organisation, Lucas Heights, New South Wales, Australia
18. Division of Environmental Science and Engineering, Pohang University of Science and Technology, Pohang, Republic of Korea
19. College of Resources and Environment, Southwest University, Chongqing 400715, China
20. Department of Ecology and Environmental Science, Umeå University, Umeå, Sweden

Supplementary Information

Supplementary note 1: South Georgia sedimentary profile (POB4)

South Georgia profile (POB4) is characterized by a (lacustrine) sediment sequence from 360 – 280cm (Fig. S1), with high mineral presence supported by high contents of mineral-origin K, Ti, Fe, Rb, Ca, Mn, and Sr. This is reflected in elevated Principal Component Analysis 1 (PCA1), representing mineral input. It is further shown in the core description with coarse and fine fibrous material, with fine-coarse sand. This sediment sequence is followed by peat initiation and establishment until the present (280 – 0cm). Chronology reconstructed by eight ^{14}C dates shows an age of ca. 8500 years (Fig. S2), with 4500 cal. yr BP at 280cm dividing sediment and peat sequences.

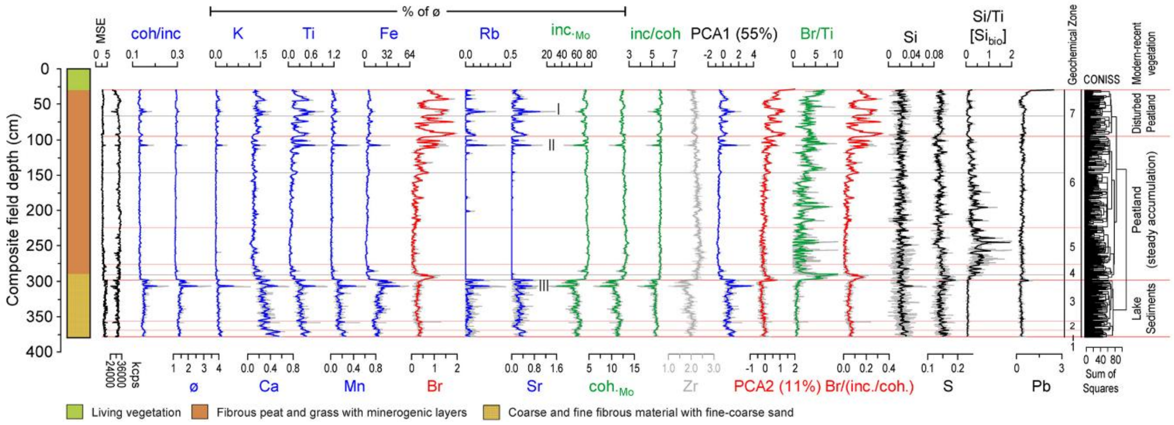

Fig. S1: Core description and mineral input in POB4 profile, with sediment and peat sequences dividing at 280cm (e.g., PCA1).

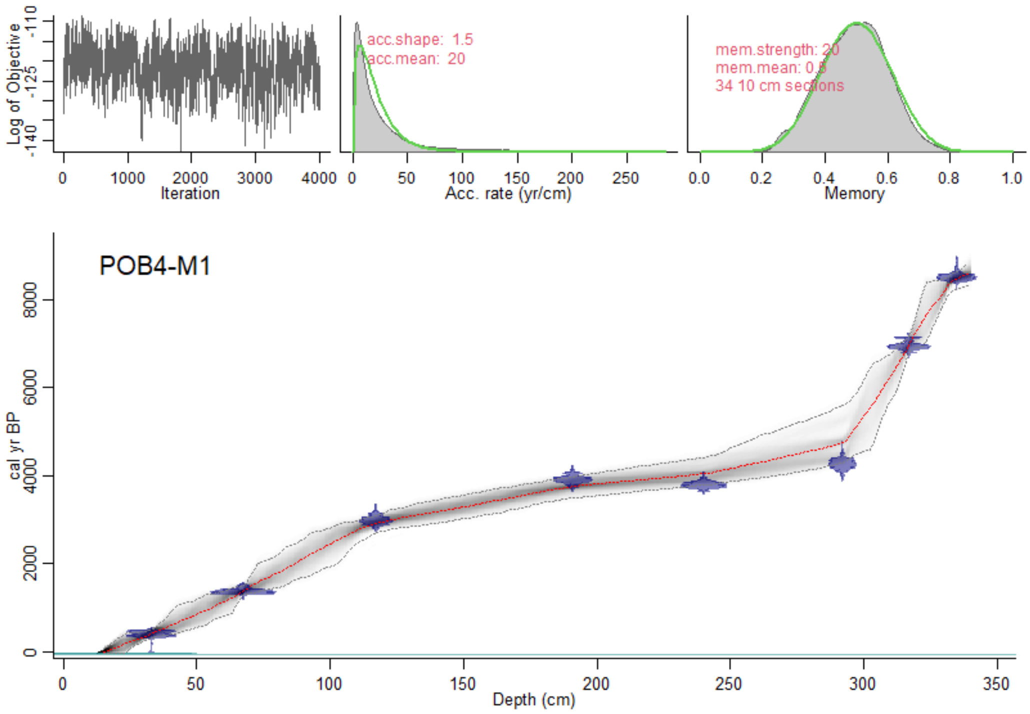

Fig. S2. Age model of POB4 core from South Georgia.

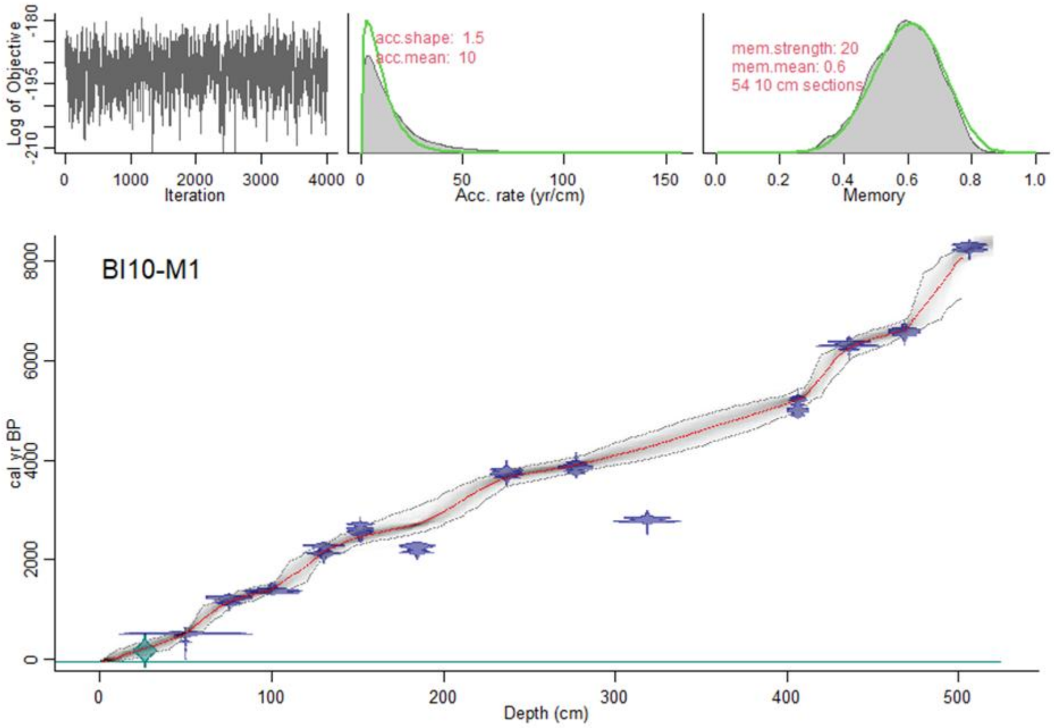

Fig. S3.Age model of BI10 core from Bird Island.

Supplementary note 2: testate amoebae productivity at Bird Island peatland BI10

The productivity of the testate amoebae community (TA) is a tracer of terrestrial salinity conditions [1], which have a direct link to the prevailing Southern Westerly Winds (SWW) to Bird Island peatland BI10. Inputs of wind-blown salt-spray deposition at the coring location can be principally tracked through their effect on the TA productivity , which is negatively related to salinization [1]. Briefly, TA were isolated from core sub-samples using a standard water-based protocol for peatlands, involving wet sieving of disaggregated material to retain particles between 15 and 300 µm [2]. Populations were quantified by direct counts at 200–400× magnification using a Zeiss AxioImager A1 light microscope, with a target of 100 individuals per sample [3]. Population density (tests cm^2 yr^{-1}), corrected for peat accumulation and temporal compression, were calculated by dividing test concentrations—derived from parallel counts with Lycopodium spores (per cm^3)—by the sample age-span inferred from the age–depth model. Detailed methods and interpretation on TA dynamics in BI10 peat cores can be found in Whittle, (2021) [4].

Supplementary note 3: Bird Island guano Hg sources

The even-Hg MIF ($\Delta^{200}Hg$ or $\Delta^{204}Hg$) is found to be exclusively generated by photochemical reactions high in the tropopause or stratosphere [5]. This implies even-Hg MIF is relatively conservative at the Earth's surface, making it a tracer of Hg sources [6,7]. Bird Island guano is characterized by a mean $\Delta^{200}Hg$ value of 0.01 ± 0.05 ‰ (2σ, n = 5), with Hg originating from two Southern Hemisphere atmospheric sources (Hg^0 $\Delta^{200}Hg$ = −0.06 ± 0.02 ‰, 1σ, n = 23; Hg^{II} $\Delta^{200}Hg$ = 0.08 ± 0.08‰, 1σ, n = 21) [8]. These two sources contribute Hg to the marine primary producers, leading to the subsequent transfer of Hg through the food web [9] to higher trophic levels, including seabirds and their by-product, guano. $\Delta^{200}Hg$ has been successfully applied to quantify the relative contributions of atmospheric Hg^0 and Hg^{II} to Hg inputs in the environments [8,10–12]. Based on the $\Delta^{200}Hg$ isotope mass balance, Bird Island guano can be explained by the oceanic Hg mixing of 47% (median; interquartile range, 28 – 68%) Hg^0 deposition and 53% (32 – 74%) atmospheric Hg^{II} contribution. This is in line with the atmospheric Hg^0 and Hg^{II} contributions estimated by the Δ^{200}Hg mixing model in a pioneering ocean Hg study [9].

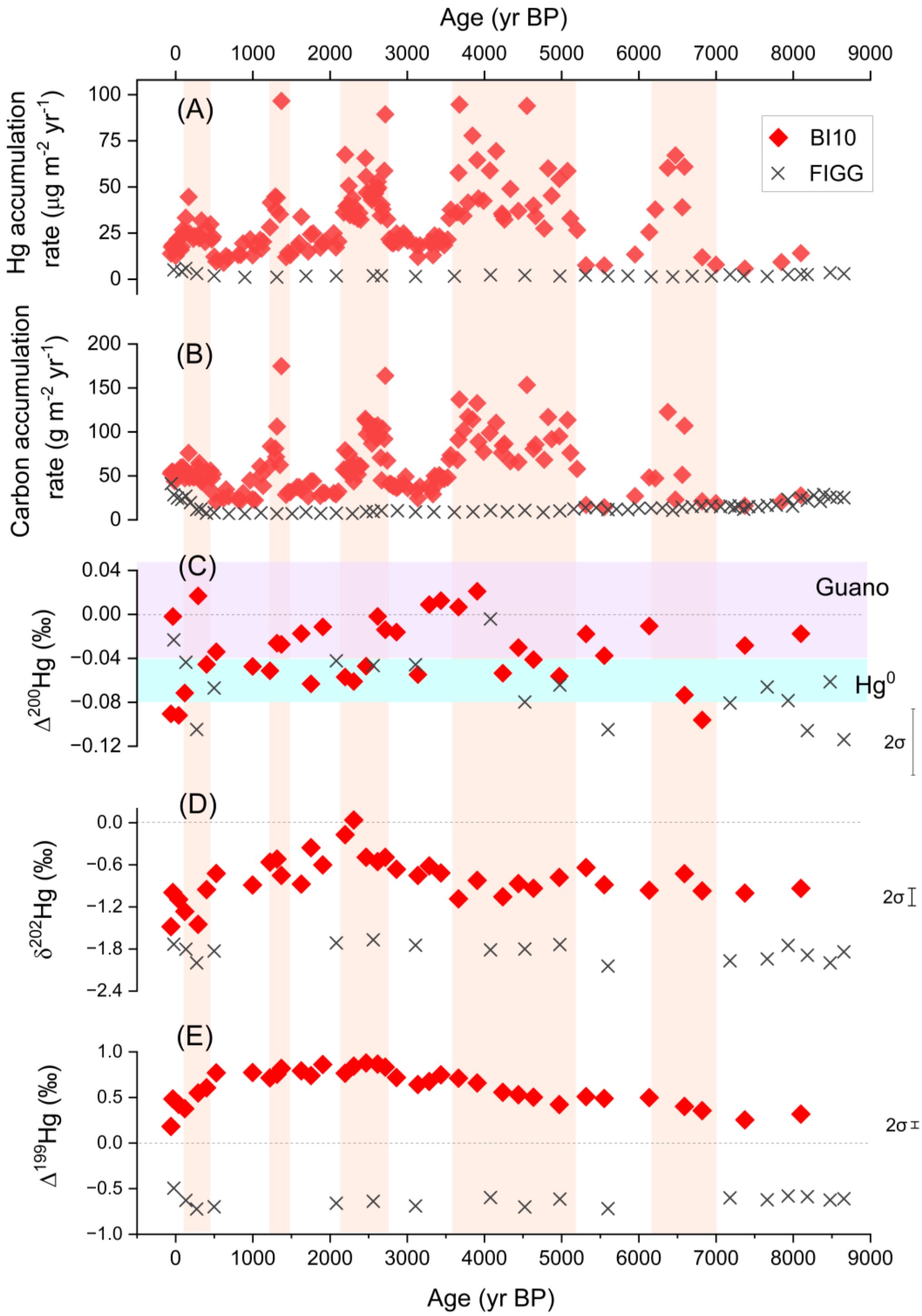

Fig. S4. Profiles of Hg accumulation rate (A), carbon accumulation rate (B), Δ^{200}Hg (C), δ^{202}Hg (D), and Δ^{199}Hg (E) in BI10 and FIGG peat cores. Orange-shaded areas highlight five periods with high Hg flux linked to enhanced guano input. In (C) Purple-shaded area represents the guano Δ^{200}Hg signature (0.01 ± 0.05 ‰, 2σ, n = 5, this study), while the green-shaded area represents the atmospheric Hg^0 (−0.06 ± 0.02 ‰, 1σ, n = 23) [8].

Supplementary note 4. Reduction processes of Hg in the Falkland Islands FIGG core.

At the reference site, FIGG peat $\Delta^{199}Hg$ were all lower than the calculated peat $\Delta^{199}Hg$ from the mass balance of the two atmospheric endmembers (i.e., atmospheric Hg^0 and rainfall Hg^{II}, Fig. S5B). The systematically more negative $\Delta^{199}Hg$ in FIGG peat as compared to the atmosphere endmembers can be explained by photochemical reduction, or dark abiotic reduction of Hg^{II} [13–15].

The slope of $\Delta^{199}Hg/\Delta^{201}Hg$ can generally inform about potential reduction processes. The associated FIGG peat slope is 1.30 ± 0.67 (1σ) based on York linear fitting considering the maximum 2σ analytical certainty of the isotopes (Fig. S5C). This slope with a large uncertainty may not be used to precisely identify the dominant reduction process, such as dark abiotic Hg reduction driven by nuclear volume fractionation ($\Delta^{199}Hg/\Delta^{201}Hg$ = 1.6 ± 0.03, 1σ) [15], and in-situ foliar Hg^{II} photoreduction ($\Delta^{199}Hg/\Delta^{201}Hg$ = 0.79 ± 0.06, 1σ) [13]. Similar large uncertainty in the slope of $\Delta^{199}Hg/\Delta^{201}Hg$ is also seen in the boreal Degero peat profiles (domed hummock, 1.29 ± 0.84, 1σ; flatter lawn, 1.75 ± 1.2, 1σ) [12]. Despite the $\Delta^{199}Hg/\Delta^{201}Hg$ slope is not used as a tracer in this boreal peatland, this study [12] clearly demonstrates that photoreduction is the dominant transformation process, liberating 30% of deposited peat Hg back to the atmosphere, while dark abiotic reduction is insignificant during peat decomposition. The insignificance of dark abiotic reduction derives from the findings of prevailing oxidation process in the peat unsaturated zone above the water table level, and photoreduction of rainfall Hg^{II} as the dominant source of the groundwater gaseous Hg^0 in the saturated zone below the water table level. This is based on a comprehensive investigation of Hg sources and sinks in different peat microforms (hummock and lawn), peat gas, and peat groundwater dissolved gaseous Hg^0. Furthermore, a litter decomposition experiment over the course of two years showed no significant change in the residual Hg^{II} $\Delta^{199}Hg$ (–0.28 ± 0.07‰ to –0.34 ± 0.07‰, 1σ, n = 8) [16], indicating there would be no significant alteration of $\Delta^{199}Hg$ during decomposition of litter and possibly the organic matter of peat. It is likely that more negative $\Delta^{199}Hg$ in FIGG peat results from photoreduction, even though we could not rule out the influence of dark abiotic Hg reduction.

Supplementary note 5: Influence of SWW on Falkland Islands seabird dynamics [17]

The seabird establishment at Falkland Island Surf Bay at c. 5 ka BP was thought to link to a possibly stronger SWW [17], which is opposite to the finding of a weaker SWW in Bird Island. These seemingly contrasting results may imply the highly dynamic nature of SWW in different regions [18] and/or the different responses of different seabird species and/or breeding habitats with different exposure to strengthened SWW [19]. It also highlights the importance of using climate records from the local areas for comparison with seabird population dynamics. This is also a future need to develop techniques to identify seabirds by species in the archives (e.g., e-DNA tool).

Supplementary note 6: Lower seabird population periods

Lower seabird populations in some periods at BI10 are unlikely to have been caused by postglacial change in sea level, as the catchment is well above the Holocene marine limit on South Georgia [20]. Therefore, we conclude that reductions in guano input, which coincide with periods of lower *testate amoebae* productivity, are most likely due to reduced seabird breeding densities, driven by unfavorable climate conditions associated with stronger SWW.

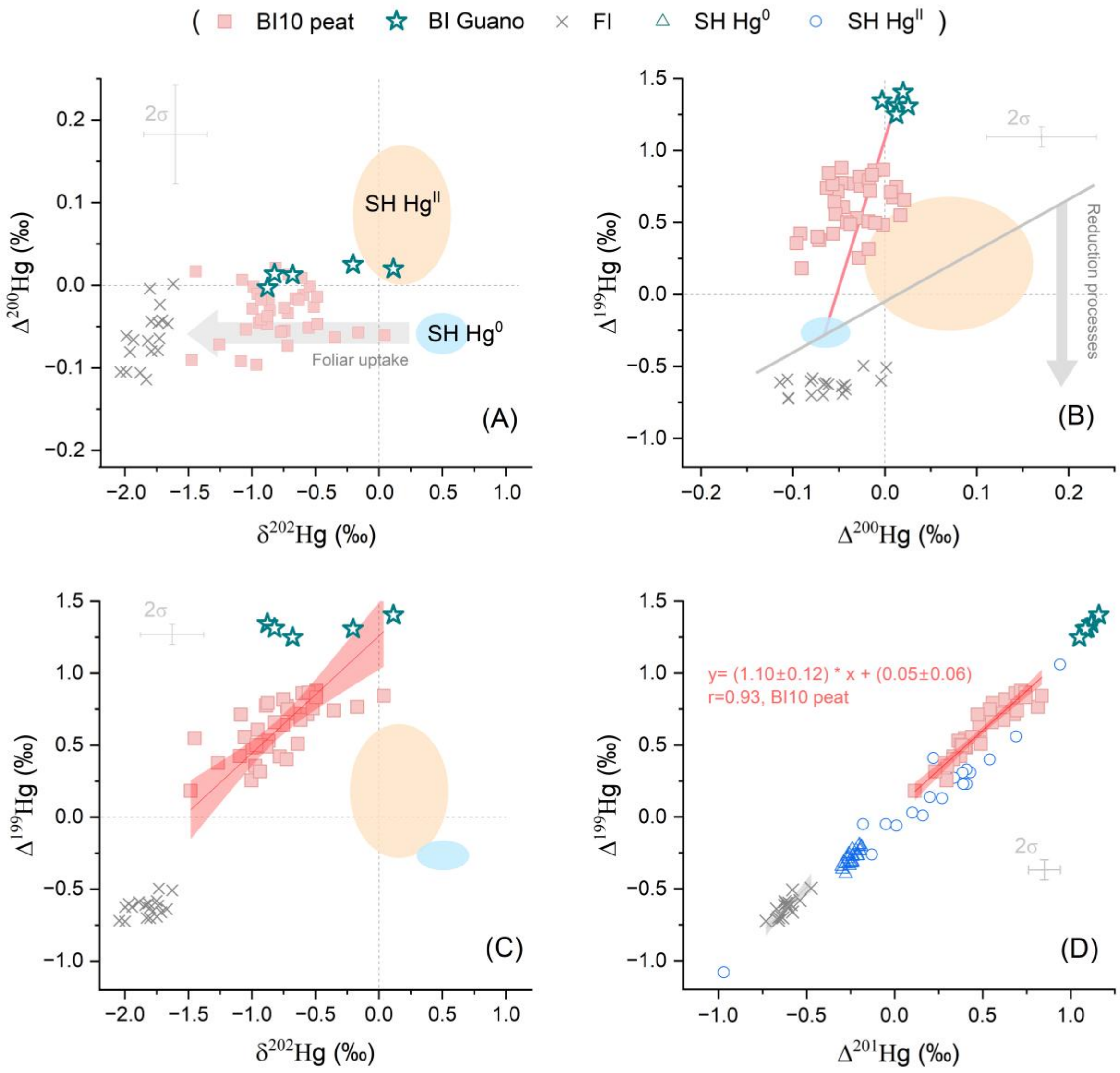

Fig. S5. A) Δ^{200}Hg vs δ^{202}Hg, (B) Δ^{199}Hg vs Δ^{200}Hg, (C) Δ^{199}Hg vs δ^{202}Hg, and (D) Δ^{199}Hg vs Δ^{201}Hg in the Bird Island BI10 peatland (pink filled squares), Bird Island guano (green open stars), Falkland Islands FIGG peatland (grey crosses), and Southern Hemisphere atmospheric Hg^0 (SH Hg^0, blue filled ellipse) and rainfall Hg^{II} (SH Hg^{II}, orange filled ellipse) [8]. Grey arrow in (A) indicates preferential foliar uptake of light isotopes from atmospheric Hg^0. In (B), the red line represents the mass balance mixing between guano and SH Hg^0. The grey line stands for the mass balance mixing between SH Hg^0 and Hg^{II}, and the grey arrow from this mixing line indicates reduction processes leaving more negative Δ^{199}Hg in residue peat samples.

Supplementary tables S1-6

Table S1. Bird Island BI10 datasets, including age (cal. yr BP), depth (cm), density (g cm-3), peat accumulation rates (g cm-2 yr-1), C content (%), carbon accumulation rates (g m-2 yr-1), Hg concentration (μg g^{-1}), Hg accumulation rates (μg m-2 yr-1), Hg/C (ng g-1), and Hg isotope composition (‰).

List	Age	Depth	Density	Peat accumulation rates	C content	Carbon accumulation rates	Hg concentration	Hg accumulation rates	Hg/C	δ^{202}Hg	Δ^{199}Hg	Δ^{200}Hg	Δ^{201}Hg
	cal. yr BP	cm	g cm-3	g cm-2 yr-1	%	g m-2 yr-1	ng g-1	μg m-2 yr-1	ng g-1	‰	‰	‰	‰
1	-61	0.6	0.11	0.012	45.3	52.66	118.9	13.8	263	-1.48	0.18	-0.09	0.12
2	-49	1.9	0.12	0.012	45.7	54.62	146.4	17.5	321				
3	-36	3.2	0.11	0.012	44.0	54.64	149.5	18.6	340	-0.99	0.48	0.00	0.41
4	-11	5.8	0.09	0.009	46.6	43.84	168.2	15.8	361				
5	1	7.1	0.10	0.011	46.5	50.81	115.2	12.6	248				
6	26	9.7	0.12	0.011	44.6	50.57	190.7	21.6	428				
7	39	11	0.13	0.011	45.9	52.67	188.3	21.6	410	-1.09	0.42	-0.09	0.37
8	66	13.6	0.13	0.013	47.1	59.45	125.9	15.9	267				
9	79	14.8	0.14	0.012	45.8	55.13	145.6	17.5	318				
10	93	16.1	0.14	0.014	41.3	59.89	184.7	26.8	447				
11	118	18.5	0.15	0.014	32.8	47.28	177.1	25.5	540	-1.27	0.38	-0.07	0.29
12	131	19.8	0.17	0.018	31.0	55.20	186.9	33.3	603				
13	168	23.5	0.18	0.020	37.7	76.09	221.0	44.6	586				
14	179	24.7	0.17	0.016	29.0	47.82	150.9	24.9	521				
15	230	29.8	0.15	0.012	40.3	48.26	182.3	21.8	453				
16	245	31	0.19	0.015	33.3	48.67	159.5	23.3	479				
17	291	34.5	0.20	0.016	38.2	59.66	153.3	24.0	402	-1.45	0.55	0.02	0.40
18	305	35.6	0.23	0.017	37.0	64.65	127.2	22.2	344				
19	335	37.9	0.28	0.021	20.3	43.54	148.4	31.8	731				
20	383	41.4	0.26	0.017	23.5	39.99	118.8	20.2	506				
21	401	42.6	0.21	0.014	38.3	54.63	190.5	27.2	498	-0.95	0.61	-0.05	0.49
22	452	46.2	0.19	0.013	42.1	55.93	223.9	29.8	532				
23	468	47.3	0.15	0.011	42.9	47.21	195.4	21.5	455				
24	484	48.4	0.18	0.012	43.4	51.85	192.1	22.9	442				

25	501	49.6	0.17	0.007	40.6	29.56	167.5	12.2	413				
26	527	50.7	0.18	0.007	30.1	20.39	140.9	9.5	468	-0.72	0.77	-0.03	0.60
27	622	54.1	0.16	0.006	41.4	24.36	150.5	8.8	363				
28	653	55.2	0.23	0.008	44.3	34.61	160.1	12.5	362				
29	687	56.4	0.16	0.006	44.7	26.62	194.1	11.6	434				
30	812	60.9	0.14	0.005	44.5	22.73	256.6	13.1	576				
31	844	62.1	0.17	0.006	33.5	21.74	203.4	13.2	607				
32	874	63.2	0.19	0.007	41.7	30.43	266.1	19.4	639				
33	965	66.6	0.31	0.011	40.3	44.82	194.7	21.7	483				
34	997	67.8	0.24	0.009	26.2	23.43	144.5	12.9	551	-0.89	0.77	-0.05	0.61
35	1027	68.9	0.28	0.011	20.2	22.24	165.7	18.2	818				
36	1095	72.4	0.23	0.014	43.2	60.76	151.9	21.4	352				
37	1114	73.6	0.19	0.012	42.2	51.40	136.0	16.6	322				
38	1133	74.8	0.18	0.011	34.8	38.56	183.0	20.3	527				
39	1221	80.5	0.17	0.017	36.2	61.25	166.2	28.1	459	-0.56	0.71	-0.05	0.68
40	1233	81.7	0.19	0.021	39.1	83.61	194.2	41.5	497				
41	1291	87.7	0.17	0.020	41.2	81.02	227.9	44.8	553				
42	1301	88.8	0.19	0.018	39.7	71.57	208.5	37.6	525				
43	1313	90	0.19	0.025	42.4	106.10	176.3	44.2	416	-0.52	0.75	-0.03	0.69
44	1351	94.5	0.24	0.029	21.7	62.30	122.4	35.1	564				
45	1370	96.8	0.35	0.044	39.3	174.79	217.3	96.6	553	-0.75	0.82	-0.03	0.63
46	1430	101.4	0.18	0.007	39.4	28.42	165.7	12.0	421				
47	1459	102.6	0.18	0.007	42.6	31.71	193.2	14.4	454				
48	1486	103.7	0.19	0.007	42.1	31.43	174.9	13.1	416				
49	1571	107.2	0.21	0.009	43.5	37.21	201.0	17.2	462				
50	1600	108.4	0.20	0.009	43.6	37.22	228.3	19.5	524				
51	1627	109.5	0.22	0.008	40.2	33.85	401.2	33.8	998	-0.88	0.79	-0.02	0.56
52	1718	113	0.19	0.006	41.3	26.61	232.8	15.0	563				
53	1753	114.3	0.25	0.010	42.5	43.87	235.6	24.3	554	-0.36	0.74	-0.06	0.70
54	1782	115.4	0.28	0.010	42.5	43.78	241.5	24.9	568				
55	1874	118.9	0.17	0.006	44.4	27.20	279.5	17.1	629				

56	1906	120.1	0.17	0.007	44.3	31.02	281.5	19.7	635	-0.60	0.86	-0.01	0.69
57	1934	121.2	0.18	0.007	44.3	30.38	294.8	20.2	666				
58	2048	125.6	0.18	0.007	42.2	30.33	345.9	24.9	820				
59	2077	126.7	0.18	0.007	42.4	28.97	251.9	17.2	593				
60	2108	127.9	0.18	0.007	43.3	32.15	274.8	20.4	635				
61	2179	131.3	0.19	0.014	41.5	57.36	261.6	36.1	630				
62	2195	132.5	0.27	0.019	42.0	79.08	358.1	67.5	853	-0.17	0.77	-0.06	0.82
63	2212	133.7	0.18	0.013	40.9	54.57	297.0	39.6	726				
64	2228	134.9	0.20	0.015	38.5	59.23	261.4	40.2	678				
65	2243	136	0.24	0.018	42.0	74.96	283.7	50.6	675				
66	2259	137.2	0.19	0.014	37.7	51.75	252.8	34.7	670				
67	2290	139.5	0.21	0.014	43.5	61.88	308.1	43.9	709				
68	2307	140.7	0.19	0.012	36.1	43.77	282.2	34.2	782	0.04	0.84	-0.06	0.84
69	2325	141.9	0.22	0.015	43.3	64.92	257.8	38.7	596				
70	2360	144.2	0.19	0.012	43.1	51.54	274.3	32.8	637				
71	2379	145.5	0.20	0.014	44.4	60.78	261.8	35.9	590				
72	2396	146.6	0.20	0.014	44.2	61.01	233.5	32.2	528				
73	2458	151.5	0.22	0.029	40.0	114.84	228.3	65.6	571				
74	2467	152.7	0.20	0.027	41.4	112.95	203.5	55.6	492	-0.49	0.88	-0.05	0.72
75	2476	153.9	0.17	0.022	44.7	97.46	215.4	46.9	481				
76	2526	160.5	0.17	0.024	43.0	104.06	191.0	46.2	444				
77	2535	161.8	0.15	0.025	43.2	106.88	179.9	44.5	416				
78	2543	163.1	0.15	0.021	42.1	86.74	208.5	42.9	495				
79	2568	166.7	0.16	0.023	43.9	100.35	216.0	49.4	493				
80	2576	167.9	0.16	0.023	41.2	95.45	201.7	46.8	490				
81	2584	169.1	0.15	0.026	41.3	105.71	181.6	46.5	440				
82	2608	172.7	0.16	0.022	42.7	93.52	221.7	48.6	520				
83	2617	173.9	0.16	0.024	44.2	107.37	217.4	52.8	492	-0.55	0.87	0.00	0.74
84	2625	175.1	0.16	0.022	42.4	93.82	223.8	49.6	528				
85	2657	179.8	0.17	0.019	38.1	70.59	185.8	34.4	488				
86	2668	181	0.20	0.020	22.2	44.87	199.5	40.4	900				

87	2680	182.2	0.28	0.029	35.6	103.62	130.1	37.9	366				
88	2704	184.7	0.25	0.025	36.2	92.04	231.3	58.8	639				
89	2716	185.9	0.42	0.042	38.9	163.94	212.0	89.4	545	-0.49	0.83	-0.01	0.75
90	2741	188.4	0.16	0.017	40.0	67.31	192.9	32.4	482				
91	2770	190.7	0.21	0.010	39.6	40.84	209.9	21.6	530				
92	2793	191.9	0.19	0.010	40.7	40.65	199.5	19.9	491				
93	2816	193.1	0.20	0.010	39.0	38.18	198.1	19.4	508				
94	2840	194.3	0.17	0.009	40.4	38.28	213.5	20.2	529				
95	2861	195.4	0.19	0.009	38.7	36.20	265.2	24.8	685	-0.66	0.72	-0.02	0.62
96	2884	196.6	0.22	0.012	31.8	37.50	167.9	19.8	528				
97	2952	200.1	0.25	0.011	36.5	40.89	222.2	24.9	608				
98	2979	201.3	0.28	0.013	38.6	49.10	181.6	23.1	470				
99	3006	202.5	0.25	0.011	33.5	35.97	194.6	20.9	580				
100	3113	207.2	0.20	0.009	36.1	33.28	198.0	18.3	549				
101	3138	208.3	0.16	0.007	33.6	24.55	165.0	12.1	491	-0.75	0.64	-0.05	0.48
102	3165	209.5	0.20	0.009	39.7	37.69	192.9	18.3	486				
103	3285	215.5	0.20	0.010	38.1	38.35	199.4	20.1	523	-0.62	0.67	0.01	0.62
104	3309	216.7	0.19	0.010	33.9	33.38	198.6	19.6	586				
105	3333	217.9	0.17	0.008	36.2	29.04	161.4	13.0	446				
106	3355	219	0.22	0.012	41.3	49.97	196.0	23.7	474				
107	3373	219.9	0.21	0.012	41.6	48.55	182.5	21.3	439				
108	3393	221	0.19	0.010	41.9	41.44	193.8	19.2	463				
109	3415	222.2	0.21	0.012	42.2	50.71	192.2	23.1	455				
110	3436	223.4	0.23	0.012	39.8	48.97	168.4	20.7	423	-0.72	0.75	0.01	0.54
111	3458	224.6	0.21	0.012	38.8	47.12	172.2	20.9	444				
112	3479	225.8	0.20	0.011	41.9	46.39	166.1	18.4	396				
113	3524	228.3	0.21	0.012	40.7	48.14	181.9	21.5	447				
114	3546	229.5	0.24	0.017	40.7	68.84	195.1	33.0	480				
115	3563	230.7	0.22	0.019	38.0	73.61	194.7	37.7	512				
116	3650	238.1	0.19	0.017	40.8	68.03	216.7	36.2	532				
117	3664	239.3	0.22	0.022	40.9	91.27	258.6	57.7	632	-1.09	0.71	0.01	0.47

118	3676	240.5	0.20	0.035	39.4	136.96	272.5	94.6	691				
119	3729	249.4	0.15	0.023	43.5	101.62	147.0	34.3	338				
120	3788	259.1	0.16	0.027	43.7	117.28	154.5	41.5	354				
121	3845	268.7	0.16	0.028	41.2	114.02	281.2	77.8	683				
122	3906	278.4	0.21	0.032	42.0	132.70	204.5	64.6	487	-0.82	0.66	0.02	0.55
123	3923	280.8	0.20	0.021	41.8	88.67	206.3	43.8	493				
124	3989	288.2	0.18	0.019	39.9	77.36	218.8	42.4	549				
125	4070	297.9	0.22	0.026	38.1	98.87	226.9	58.9	596				
126	4152	307.6	0.29	0.036	30.3	110.37	190.5	69.4	629				
127	4227	316.2	0.18	0.020	38.2	76.15	178.1	35.5	467				
128	4238	317.5	0.18	0.021	41.0	84.35	166.9	34.3	407	-1.06	0.56	-0.05	0.44
129	4260	320	0.20	0.021	41.1	86.47	153.3	32.3	373				
130	4336	327.5	0.17	0.017	39.5	66.59	290.3	48.9	734				
131	4440	337.2	0.20	0.017	38.4	65.63	216.4	37.0	564	-0.87	0.53	-0.03	0.36
132	4550	347.2	0.54	0.048	32.0	153.37	195.7	93.9	613				
133	4635	354.7	0.22	0.021	38.8	80.54	192.1	39.9	495	-0.93	0.50	-0.04	0.38
134	4663	357.2	0.27	0.023	37.9	85.53	151.5	34.2	400				
135	4775	367	0.22	0.018	39.0	68.26	157.0	27.5	403				
136	4825	371.6	0.29	0.030	38.5	116.95	197.5	60.1	514				
137	4871	376.4	0.25	0.026	35.7	91.72	176.2	45.2	493				
138	4970	385.9	0.26	0.024	39.7	95.07	226.8	54.3	571	-0.78	0.42	-0.06	0.34
139	5076	395.8	0.31	0.029	39.4	113.53	203.3	58.6	517				
140	5114	399.4	0.26	0.021	36.4	76.15	157.2	32.8	431				
141	5200	405.3	0.23	0.015	38.7	57.86	178.0	26.6	460				
142	5316	410.9	0.22	0.005	37.3	16.81	167.8	7.6	449	-0.64	0.51	-0.02	0.49
143	5552	415.7	0.19	0.004	38.2	14.29	200.3	7.5	524	-0.88	0.49	-0.04	0.40
144	5951	425.5	0.24	0.007	38.8	26.97	192.8	13.4	497				
145	6134	431.4	0.26	0.012	40.2	48.21	212.2	25.5	528	-0.96	0.50	-0.01	0.39
146	6213	435	0.29	0.012	38.9	47.12	312.2	37.8	802				
147	6375	445	0.30	0.029	41.9	122.63	206.2	60.4	492				
148	6474	454.4	0.54	0.049	4.7	22.95	137.6	67.1	2925				

149	6562	462.2	0.23	0.020	25.4	51.16	193.4	39.0	762				
150	6591	464.7	0.45	0.037	28.7	107.00	163.5	61.0	570	-0.73	0.40	-0.07	0.33
151	6820	473.6	0.27	0.006	34.9	21.04	197.0	11.9	565	-0.97	0.36	-0.10	0.30
152	6999	477.5	0.25	0.005	34.4	18.89	142.9	7.8	415				
153	7373	486	0.16	0.004	42.1	15.93	151.2	5.7	359	-1.00	0.25	-0.03	0.30
154	7847	496.6	0.24	0.005	39.3	20.55	176.9	9.3	450				
155	8099	504.5	0.16	0.008	36.6	27.67	186.3	14.1	509	-0.94	0.32	-0.02	0.23

Table S2. Falkland Islands FIGG datasets, including age (cal. yr BP), depth (cm), density (g cm-3), peat accumulation rates (g cm-2 yr-1), C content (%), carbon accumulation rates (g m-2 yr-1), Hg concentration (µg g^{-1}), Hg accumulation rates (µg m-2 yr-1), Hg/C (ng g-1), and Hg isotope composition (‰).

List	Age	Depth	Density	Peat accumulation rates	C content	Carbon accumulation rates	Hg concentration	Hg accumulation rates	Hg/C	δ^{202}Hg	Δ^{199}Hg	Δ^{200}Hg	Δ^{201}Hg
	cal. yr BP	cm	g cm-3	g cm-2 yr-1	%	g m-2 yr-1	ng g-1	µg m-2 yr-1	ng g-1	‰	‰	‰	‰
1	-57	3.02	0.124	0.010	41.5	41.2							
2	-24	5.54	0.130	0.007	43.1	28.5	76.3	5.0	176.8	-1.73	-0.50	-0.02	-0.47
3	23	8.06	0.132	0.006	42.6	24.7							
4	78	10.60	0.113	0.005	43.6	23.2	77.4	4.1	177.3				
5	133	13.11	0.134	0.006	43.5	26.9	95.4	5.9	219.6	-1.80	-0.63	-0.04	-0.60
6	191	15.58	0.124	0.005	41.1	19.6							
7	272	17.98	0.131	0.003	42.8	11.6	113.8	3.1	266.1	-2.00	-0.724	-0.105	-0.731
8	328	19.20	0.139	0.003	40.1	12.1							
9	399	20.42	0.153	0.002	39.7	7.6							
10	498	21.65	0.147	0.002	40.0	8.2	88.9	1.8	222.2	-1.83	-0.70	-0.07	-0.66
11	690	24.17	0.135	0.002	41.2	6.7							
12	896	26.69	0.133	0.002	43.9	6.8	69.7	1.1	159.0				
13	1105	29.25	0.149	0.002	42.4	8.0							
14	1310	31.74	0.131	0.002	43.9	6.8	72.4	1.1	164.9				
15	1509	34.19	0.145	0.002	40.8	6.9							

16	1688	36.64	0.145	0.002	40.9	8.8	78.0	1.7	190.6				
17	1878	39.08	0.164	0.002	36.8	7.2							
18	2081	41.62	0.171	0.002	37.1	7.7	85.7	1.8	231.1	-1.71	-0.660	-0.042	-0.580
19	2290	44.19	0.163	0.002	35.8	6.9							
20	2468	46.77	0.158	0.002	39.9	9.2							
21	2560	48.04	0.172	0.002	43.3	9.3	87.3	1.9	201.8	-1.67	-0.64	-0.05	-0.67
22	2666	49.33	0.188	0.002	44.0	10.5	78.1	1.9	177.3				
23	2873	51.84	0.197	0.002	42.1	10.3							
24	3107	54.35	0.195	0.002	43.6	9.0	72.6	1.5	166.4	-1.75	-0.69	-0.05	-0.65
25	3345	56.85	0.197	0.002	42.0	9.0							
26	3610	59.34	0.213	0.002	43.6	8.6	80.9	1.6	185.5				
27	3852	61.76	0.253	0.003	35.3	9.2							
28	4078	64.23	0.265	0.003	37.0	10.8	78.8	2.3	213.2	-1.81	-0.60	0.00	-0.60
29	4297	66.72	0.266	0.003	32.6	9.1							
30	4523	69.24	0.218	0.002	43.5	10.6	83.4	2.0	192.0	-1.80	-0.701	-0.080	-0.635
31	4761	71.70	0.209	0.002	43.3	8.5							
32	4977	74.14	0.190	0.002	45.6	10.1	77.6	1.7	170.0	-1.74	-0.61	-0.06	-0.62
33	5158	76.60	0.206	0.003	39.2	12.2							
34	5308	79.03	0.191	0.003	42.3	14.0	66.5	2.2	157.1				
35	5448	81.43	0.174	0.003	48.2	13.9							
36	5600	83.84	0.167	0.003	45.9	11.6	64.2	1.6	139.9	-2.04	-0.72	-0.10	-0.66
37	5710	85.43	0.173	0.003	44.0	12.1							
38	5858	87.81	0.164	0.003	42.5	11.6	66.5	1.8	156.4				
39	6001	90.18	0.175	0.003	45.5	13.3							
40	6159	92.61	0.167	0.003	48.5	13.2	51.7	1.4	106.5				
41	6305	95.01	0.183	0.003	43.1	13.6							
42	6439	97.38	0.148	0.003	43.6	10.9	52.2	1.3	119.8				
43	6562	99.81	0.163	0.003	42.2	14.0							
44	6690	102.24	0.179	0.004	41.5	15.1	45.8	1.7	110.4				
45	6812	104.63	0.190	0.004	40.8	15.6							
46	6940	107.05	0.170	0.003	46.6	15.8	50.8	1.7	108.9				

47	7058	109.44	0.175	0.003	43.7	14.9							
48	7181	111.78	0.192	0.004	43.3	15.6	67.2	2.4	155.2	-1.97	-0.60	-0.08	-0.62
49	7240	112.90	0.164	0.003	43.4	13.9							
50	7299	114.04	0.185	0.004	42.3	16.0							
51	7357	115.21	0.145	0.003	44.9	12.0	62.7	1.7	139.7				
52	7424	116.40	0.171	0.003	47.6	15.1							
53	7546	118.83	0.168	0.003	42.2	14.7							
54	7662	121.24	0.179	0.004	44.4	16.5	40.3	1.5	90.7	-1.94	-0.62	-0.07	-0.61
55	7779	123.65	0.190	0.004	42.7	16.8							
56	7933	126.86	0.257	0.005	45.9	23.1	49.1	2.5	107.0	-1.75	-0.581	-0.078	-0.537
57	7991	128.12	0.174	0.005	34.6	15.5							
58	8098	130.69	0.176	0.005	50.0	24.8	53.1	2.6	106.1				
59	8182	133.15	0.162	0.005	48.0	22.1	54.2	2.5	112.9	-1.89	-0.588	-0.106	-0.621
60	8266	135.70	0.180	0.005	53.1	27.7							
61	8351	138.20	0.153	0.004	48.0	21.0							
62	8393	139.42	0.185	0.006	49.5	28.8							
63	8477	141.88	0.194	0.006	45.5	25.8	61.8	3.5	135.8	-2.00	-0.62	-0.06	-0.61
64	8567	144.41	0.199	0.005	47.4	25.6							
65	8655	146.92	0.187	0.006	44.8	25.0	53.0	3.0	118.5	-1.84	-0.61	-0.11	-0.59

Table S3. South Georgia POB4 datasets, including age (cal. yr BP), depth (cm), density (g cm-3), peat accumulation rates (g cm-2 yr-1), C content (%), carbon accumulation rates (g m-2 yr-1), Hg concentration (µg g^{-1}), Hg accumulation rates (µg m-2 yr-1), Hg/C (ng g-1),

Age	Depth	Density	Peat accumulation rates	C content	Carbon accumulation rates	Hg concentration	Hg accumulation rates	Hg/C
cal. yr BP	cm	g cm-3	g cm-2 yr-1	%	g m-2 yr-1	ng g-1	µg m-2 yr-1	ng g-1
-12.8	15.7	0.041	0.002	49.5	8.8	39	0.7	79.6
19.1	17.0	0.079	0.003	49.0	16.7	38	1.3	77.0
51.0	18.5	0.098	0.005	48.7	22.1	35	1.6	72.5

82.9	19.9	0.079	0.003	49.0	16.7	33	1.1	68.2
117.1	21.4	0.104	0.004	48.6	21.7	38	1.7	78.8
151.3	22.9	0.123	0.005	48.0	25.2	39	2.1	81.7
185.9	24.3	0.114	0.005	48.1	25.0	46	2.4	94.8
216.2	25.7	0.080	0.003	48.2	16.2	55	1.9	115.0
248.8	27.1	0.110	0.005	47.9	22.2	66	3.0	136.8
281.4	28.5	0.094	0.004	47.9	19.1	86	3.4	179.5
316.4	29.9	0.151	0.007	48.3	33.2	92	6.3	189.3
415.6	34.0	0.055	0.002	48.0	9.8	81	1.7	169.1
483.0	36.8	0.354	0.014	40.4	54.6	77	10.5	191.3
563.3	39.9	0.388	0.015	30.0	44.4	62	9.2	207.0
683.3	44.4	0.472	0.019	32.0	59.7	56	10.4	174.5
847.3	50.5	0.244	0.009	45.5	40.8	54	4.9	118.9
1057.2	58.1	0.544	0.018	31.6	56.3	82	14.6	259.2
1138.8	61.1	0.675	0.023	32.5	74.5	57	13.1	175.8
1274.4	65.4	0.376	0.010	38.2	37.3	64	6.3	168.4
1377.5	68.2	0.226	0.006	41.3	26.0	65	4.1	157.4
1480.6	70.9	0.335	0.009	44.4	41.5	55	5.2	124.7
1611.9	74.6	0.415	0.015	38.6	56.9	48	7.1	124.6
1646.6	75.9	0.199	0.007	29.8	19.5	68	4.5	229.4
1687.2	77.3	0.382	0.014	45.5	61.6	66	8.9	144.6
1843.5	82.8	0.170	0.006	45.3	24.9	64	3.5	142.2
2037.0	88.3	0.239	0.006	37.2	23.8	54	3.5	146.2
2232.1	93.8	0.581	0.019	25.8	48.9	62	11.8	240.9
2276.0	95.2	0.317	0.010	27.3	28.2	74	7.6	269.9
2320.0	96.6	0.436	0.013	35.7	47.2	72	9.5	201.3
2401.6	99.3	0.133	0.004	44.3	19.9	64	2.9	143.6
2567.1	104.5	0.336	0.011	43.5	48.8	58	6.5	134.1
2609.7	106.0	0.196	0.007	42.5	27.7	67	4.3	156.4
2743.5	110.3	0.441	0.015	42.8	63.1	44	6.6	103.9
2828.7	113.2	0.298	0.014	37.7	53.2	48	6.8	128.6

2907.0	117.7	0.141	0.009	39.1	36.3	55	5.1	140.5
2979.4	122.3	0.575	0.039	46.5	*180.0*	38	14.7	81.7
2999.0	123.7	0.246	0.022	19.6	44.0	39	8.7	198.6
3140.6	136.6	0.448	0.043	44.3	192.3	49	21.4	111.2
3242.9	146.2	0.225	0.021	36.1	75.0	46	9.5	127.2
3306.3	151.9	0.140	0.012	45.5	53.9	45	5.4	99.8
3331.2	154.0	0.222	0.019	40.8	77.7	46	8.7	111.6
3425.5	161.9	0.119	0.010	46.3	47.4	35	3.6	75.2
3588.0	175.7	0.116	0.010	44.0	45.1	30	3.1	68.4
3666.6	182.4	0.283	0.025	45.7	115.4	36	9.2	79.6
3702.4	186.2	0.105	0.011	46.6	51.3	29	3.1	61.3
3714.6	187.5	0.183	0.019	46.8	89.9	28	5.4	60.0
3776.7	194.3	0.086	0.016	47.2	75.7	30	4.8	63.5
3813.3	200.7	0.196	0.034	42.8	145.0	45	15.3	105.7
3842.5	205.9	0.112	0.019	46.6	89.6	43	8.2	91.9
3866.1	209.9	0.184	0.032	47.0	149.1	42	13.2	88.5
3912.9	218.1	0.106	0.018	45.1	83.1	43	7.8	94.3
3955.9	225.7	0.160	0.026	47.8	124.3	29	7.5	60.5
3999.2	233.0	0.123	0.020	47.4	93.6	29	5.7	61.1
4050.1	240.6	0.083	0.012	47.8	59.4	34	4.2	70.2
4130.9	248.1	0.107	0.008	44.6	33.8	39	3.0	88.0
4214.7	254.3	0.094	0.007	44.6	31.4	37	2.6	81.9
4313.6	262.2	0.162	0.013	45.3	57.7	48	6.1	106.5
4415.2	269.8	0.099	0.007	47.3	34.6	30	2.2	63.2
4553.8	279.8	0.126	0.009	35.6	32.3	46	4.1	128.0
4700.2	289.9	0.349	0.023	35.9	81.5	45	10.2	124.6
4721.7	291.2	0.191	0.012	35.8	44.4	47	5.8	131.3
5111.5	297.9	0.444	0.005	21.6	11.4	55	2.9	252.2
5313.2	300.3	0.260	0.003	32.8	10.0	97	3.0	296.4
5548.5	303.0	0.432	0.005	28.2	13.1	68	3.2	241.2
5819.4	305.9	0.243	0.002	31.7	7.9	100	2.5	314.8

6097.4	308.8	0.778	0.008	8.3	6.6	59	4.7	711.7
6231.6	310.2	0.402	0.004	24.5	10.1	116	4.8	474.0
6365.8	311.6	0.551	0.006	15.2	9.2	99	6.0	653.1
6653.1	314.5	0.314	0.003	33.1	9.6	91	2.6	274.0
7078.2	318.5	0.446	0.004	27.7	11.4	77	3.2	278.8
7375.8	321.3	0.309	0.003	23.7	7.2	105	3.2	444.3
7899.8	327.0	0.327	0.004	29.6	12.4	115	4.8	390.3
8351.9	332.5	0.296	0.004	26.7	11.1	95	4.0	356.4
8577.8	339.4	0.250	0.010	28.1	29.4	85	8.9	301.3

Table S4. Hg concentration (μg g^{-1}) and Hg isotope composition (‰) in Bird Island Albatross guano. Detailed analytical uncertainties are shown in Table S1.

Sample	c(Hg) / μg g^{-1}	δ^{202}Hg / ‰	Δ^{199}Hg / ‰	Δ^{200}Hg / ‰	Δ^{201}Hg / ‰	Δ^{204}Hg / ‰
RO25	12.7	-0.88	1.35	0.00	1.12	0.00
BF45	16.2	0.11	1.40	0.02	1.16	0.03
RB10	21.6	-0.82	1.31	0.01	1.10	-0.08
OB49	1.2	-0.20	1.31	0.03	1.09	-0.06
RV92	10.4	-0.68	1.25	0.01	1.05	-0.03

Table S5. AMS ^{14}C dating of plant macrofossils in South Georgia POB4 Core.

Lab code	Top depth (cm)	Material dated	^{14}C age (yr BP)	Calibrated age[1] (median, yr, BP)	Calibrated age with ≥95.4% probability (BP)
LuS-12478	33.1	Plant macrofossils	395 ± 40	414	319 – 508
LuS-12479	67.5	Plant macrofossils	1525 ± 40	1367	1294 – 1517
LuS-12480	117.1	Plant macrofossils	2895 ± 45	2910	2700 – 3083
LuS-12481	190.8	Plant macrofossils	3640 ± 40	3743	3493 – 3968
Beta-516807	240	Plant macrofossils	3550 ± 30	4042	3790 – 4413
LuS-12482	291.9	Plant macrofossils	3890 ± 50	4713	4290 – 5590
Beta-516808	316.7	Plant macrofossils	6120 ± 30	6941	6789 – 7149
LuS-12483	334.7	Plant macrofossils	7780 ± 50	8483	8237 – 8635
Beta-271303	379	Plant macrofossils	8110 ± 50	9046	8791 – 9353

[1]Calibrated median age is derived from age-depth modeling performed with Bacon [23].

Table S6. Hg isotopic composition of reference materials: ETH-Fluka, UM-Almaden and Apple leaves.

Standard Type	Name	n	δ^{202}Hg / ‰	Δ^{199}Hg / ‰	Δ^{200}Hg / ‰	Δ^{201}Hg / ‰	Δ^{204}Hg / ‰	*Ref*
Secondary standard	UM-Almaden	70	**-0.56**	**-0.03**	**0.01**	**-0.05**	**0.00**	Demers et al., 2013; Scanlon et al., 2020 ; Li et al., 2023
	2σ		0.13	0.07	0.05	0.08	0.13	
	ETH-Fluka	9	**-1.47**	**0.08**	**0.02**	**0.03**	**0.00**	
	2σ		0.16	0.07	0.06	0.07	0.09	
Procedural standard (Purge and Trap)	Apple Leaves (NIST SRM1515)	35	**-2.57**	**0.05**	**-0.02**	**-0.02**	**0.06**	
	2σ		0.25	0.07	0.05	0.09	0.17	

Notes: n for UM-Almaden and ETH-Fluka is the number of analyses during four sessions from April 2023 to July 2024. n for Apple Leaves is the number of preparations of the materials for purging and trapping. 2σ shows 2SD of the average of two sessions. The analytical performance on standards is well in line with published values [12,21,22].

References:

1. Whittle, A. *et al.* Salt-Enrichment Impact on Biomass Production in a Natural Population of Peatland Dwelling Arcellinida and Euglyphida (Testate Amoebae). *Microb. Ecol.* **78**, 534–538 (2019).
2. Booth, R. K., Lamentowicz, M. & Charman, D. J. Preparation and analysis of testate amoebae in peatland palaeoenvironmental studies. *Mires Peat* **7**, (2010).
3. Payne, R. J. & Mitchell, E. A. D. How many is enough? Determining optimal count totals for ecological and palaeoecological studies of testate amoebae. *J. Paleolimnol.* **42**, 483–495 (2009).
4. Whittle, A. Late Quaternary changes in the Westerly Winds over the Southern Ocean. (University of Exeter, 2021).
5. Saiz-Lopez, A. *et al.* Role of the stratosphere in the global mercury cycle. *Sci. Adv.* **11**, eads1459 (2025).
6. Blum, J. D., Sherman, L. S. & Johnson, M. W. Mercury Isotopes in Earth and Environmental Sciences. *Annu. Rev. Earth Planet. Sci.* **42**, 249–269 (2014).
7. Chen, J., Hintelmann, H., Feng, X. & Dimock, B. Unusual fractionation of both odd and even mercury isotopes in precipitation from Peterborough, ON, Canada. *Geochim. Cosmochim. Acta* **90**, 33–46 (2012).
8. Li, C. *et al.* A peat core Hg stable isotope reconstruction of Holocene atmospheric Hg deposition at Amsterdam Island (37.8oS). *Geochim. Cosmochim. Acta* **341**, 62–74 (2023).
9. Jiskra, M. *et al.* Mercury stable isotopes constrain atmospheric sources to the ocean. *Nature* **597**, 678–682 (2021).
10. Enrico, M. *et al.* Atmospheric Mercury Transfer to Peat Bogs Dominated by Gaseous Elemental Mercury Dry Deposition. *Environ. Sci. Technol.* **50**, 2405–2412 (2016).
11. Woerndle, G. E. *et al.* New Insights on Ecosystem Mercury Cycling Revealed by Stable Isotopes of Mercury in Water Flowing from a Headwater Peatland Catchment. *Environ. Sci. Technol.* **52**, 1854–1861 (2018).
12. Li, C. *et al.* Mercury deposition and redox transformation processes in peatland constrained by mercury stable isotopes. *Nat. Commun.* **14**, 7389 (2023).
13. Yuan, W. *et al.* Stable Isotope Evidence Shows Re-emission of Elemental Mercury Vapor Occurring after Reductive Loss from Foliage. *Environ. Sci. Technol.* **53**, 651–660 (2019).
14. Zheng, W. & Hintelmann, H. Isotope Fractionation of Mercury during Its Photochemical Reduction by Low-Molecular-Weight Organic Compounds. *J. Phys. Chem. A* **114**, 4246–4253 (2010).
15. Zheng, W. & Hintelmann, H. Nuclear Field Shift Effect in Isotope Fractionation of Mercury during Abiotic Reduction in the Absence of Light. *J. Phys. Chem. A* **114**, 4238–4245 (2010).
16. Yuan, W. *et al.* Stable Mercury Isotope Transition during Postdepositional Decomposition of Biomass in a Forest Ecosystem over Five Centuries. *Environ. Sci. Technol.* **54**, 8739–8749 (2020).
17. Groff, D. V. *et al.* Seabird establishment during regional cooling drove a terrestrial ecosystem shift 5000 years ago. *Sci. Adv.* **6**, eabb2788 (2020).
18. Lamy, F. *et al.* Holocene changes in the position and intensity of the southern westerly wind belt. *Nat. Geosci.* **3**, 695–699 (2010).
19. Thorne, L., Clay, T., Phillips, R., Silvers, L. & Wakefield, E. Effects of wind on the movement, behavior, energetics, and life history of seabirds. *Mar. Ecol. Prog. Ser.* **723**, 73–117 (2023).

20. Lambeck, K., Rouby, H., Purcell, A., Sun, Y. & Sambridge, M. Sea level and global ice volumes from the Last Glacial Maximum to the Holocene. *Proc. Natl. Acad. Sci.* **111**, 15296–15303 (2014).
21. Demers, J. D., Blum, J. D. & Zak, D. R. Mercury isotopes in a forested ecosystem: Implications for air-surface exchange dynamics and the global mercury cycle: MERCURY ISOTOPES IN A FORESTED ECOSYSTEM. *Glob. Biogeochem. Cycles* **27**, 222–238 (2013).
22. Scanlon, T. M. *et al.* Mercury Accumulation in Tree Rings: Observed Trends in Quantity and Isotopic Composition in Shenandoah National Park, Virginia. *J. Geophys. Res. Biogeosciences* **125**, (2020).
23. Blaauw, M. & Christen, J. A. Flexible paleoclimate age-depth models using an autoregressive gamma process. *Bayesian Anal.* **6**, (2011).